

Optics Letters

Experimental demonstration of 20 Gbit/s data encoding and 2 ns channel hopping using orbital angular momentum modes

ASHER J. WILLNER,^{1,*} YONGXIONG REN,¹ GUODONG XIE,¹ ZHE ZHAO,¹ YINWEN CAO,¹ LONG LI,¹ NISAR AHMED,¹ ZHE WANG,¹ YAN YAN,¹ PEICHENG LIAO,¹ CONG LIU,¹ MOHAMMAD MIRHOSSEINI,² ROBERT W. BOYD,² MOSHE TUR,³ AND ALAN E. WILLNER¹

¹Department of Electrical Engineering, University of Southern California, Los Angeles, California 90089, USA

²Department of Physics and Astronomy, The Institute of Optics, University of Rochester, Rochester, New York 14627, USA

³School of Electrical Engineering, Tel Aviv University, Ramat Aviv 69978, Israel

*Corresponding author: willner@usc.edu

Received 15 October 2015; revised 25 October 2015; accepted 26 October 2015; posted 27 October 2015 (Doc. ID 252021); published 11 December 2015

We explore the use of the spatial domain as a degree of freedom for data encoding and channel hopping. We experimentally demonstrate data encoding at 20 Gbit/s using four possible orbital angular momentum (OAM) modes. The influence of mode spacing and time misalignment between modal channels on the switching crosstalk and bit-error rates is investigated. We find that the use of adjacent modes with a mode spacing of one introduces an extra power penalty of 3.2 dB compared with a larger mode spacing. Moreover, we demonstrate reconfigurable hopping of a 100 Gbit/s quadrature-phase-shift-keying (QPSK) data channel between four OAM modes with a 2 ns switching guard time. The results show that the power penalties for different hopping rates and mode spacings are less than 5.3 dB. © 2015 Optical Society of America

OCIS codes: (200.6715) Switching; (060.4080) Modulation; (060.4510) Optical communications.

<http://dx.doi.org/10.1364/OL.40.005810>

Over the past few years, there has been significant interest in using the spatial domain for optical systems and networks [1,2]. Specifically, space-division multiplexing of multiple independent data streams can enable a dramatic increase in system transmission capacity [3–5]. In addition to capacity, the space domain can also enable: (i) data encoding such that the wave can occupy one of many possible space-domain values and is analogous to different values of amplitude and phase encoding [6,7] and (ii) channel hopping in reconfigurable multiaccess networking such that a switch can route data streams based on the specific spatial mode that a channel occupies [2,8–10].

In general, data can be encoded on the amplitude, phase, or temporal position of the optical wave [6,11,12]. Importantly, there are environments for which ever-more information is desired for a given amount of energy, especially in low optical

signal power scenarios [13,14]. This can be accomplished if there are more degrees of freedom that the wave can occupy and be encoded with information to provide higher energy efficiency for a given capacity (i.e., bits/photon) for either classical or quantum communications [13].

One example of enabling multiple spatial values is through the use of an orthogonal modal basis set for which the wave can occupy one of many modes at a given time. These modes can be spatially overlapping, and a possible basis set is orbital-angular-momentum (OAM) [15]. A beam can carry OAM if the phase front “twists” in a helical fashion as it propagates. The rate of twisting ℓ , an unbounded integer, is the number of 2π phase shifts in the beam’s azimuthal direction, and the beam has a donut-shaped intensity with a null in the center [16]. The OAM modes with different ℓ values are mutually orthogonal, which allows them to be efficiently (de-)multiplexed with low inherent intermodal crosstalk [16]. OAM has been used for the simultaneous transmission of multiple data-carrying beams in both free-space and specialty fiber links [5,17–19].

Alternatively, OAM can provide many discrete states for data encoding and channel hopping [20,21]. Recent work has shown OAM-based data encoding, at a 4 kHz rate using a digital micromirror device to switch between modes [14,21]. Moreover, switching based on spatial mode has been shown with switching rates limited by the programmable device [22].

In this Letter, we use different OAM modes as a basis for classical data encoding and channel hopping. For data encoding, the optical beam occupies one of four possible OAM modes, thereby doubling the information for the same amount of energy as two states. We demonstrate 20 Gbit/s encoding using a set of lithium-niobate switches. Using the same switches, we also demonstrate channel hopping in which a 100 Gbit/s quadrature-phase-shift-keying (QPSK) channel “hops” between four different modes with a 2 ns switching guard time.

Figure 1 illustrates the concept of data encoding and channel hopping using OAM modes. For data encoding, the OAM

mode selection module functions as a data modulator. It encodes bits on a continuous wave (CW) laser by converting the light into one mode in the set of $\{\ell_1, \ell_2, \ell_3, \text{ and } \ell_4\}$ for each symbol period T . Therefore, the light beam occupies one of N possible modes and the number of information bits encoded equals $\log_2 N$. Symbols can be recovered by identifying the value ℓ in each symbol period. For channel hopping, the hopping controller places the data signal on single OAM mode on the set of $\{\ell_1, \ell_2, \ell_3, \text{ and } \ell_4\}$ for a certain extended period of time. The OAM value and time duration of the data channel depend on the controller signal. To ensure the recovery of the entire transmitted data stream, a guard time that is directly related to the switching transition time is required during the process of mode hopping.

Here we demonstrate high-speed data encoding and channel hopping in free space using four OAM modes. Figure 2(a) shows the experimental setup. For OAM-based data encoding, 1550 nm CW laser light is input to Port A of a 2×4 optical “switch” that can operate at a switching rate up to 10 GHz. This “switch” is built by cascading one 2×2 optical switch with two 1×2 optical switches. Two pseudo-random bit sequences are used to drive the 2×4 “switch,” which allows the CW light to be routed to one of the four output paths. Specially, the mapping relation between the two sequences and out ports is $00 \rightarrow \textcircled{1}$, $01 \rightarrow \textcircled{2}$, $11 \rightarrow \textcircled{3}$, and $10 \rightarrow \textcircled{4}$. Tunable delay lines are inserted into the parallel paths for synchronization. For OAM channel hopping, a 100 Gbit/s QPSK signal at 1550 nm is amplified and split into two copies, one of which is delayed using a single mode fiber for de-correlation. The two

copies are sent to Ports A and B of the 2×4 “switch.” Each of the output branches of the switch is sent to a free-space collimator with a diameter of 3 mm and launched onto a programmable spatial light modulator (SLM). Each SLM is loaded with a specific spiral phase hologram to convert a beam into a desired OAM value in the set of $\{\ell_1, \ell_2, \ell_3, \text{ and } \ell_4\}$. Figure 2(b) shows the intensity profiles (b1–b4) and interferograms (b5–b8) of four different OAM beams $\ell = -3, -1, +1, \text{ and } +3$, with a mode spacing $\Delta = 2$. The interferograms are obtained from interfering OAM beams with an expanded Gaussian beam. We see that the rotating arms in Figs. 2(b5)–2(b8) confirm the OAM value of each beam.

Sequentially, four branches are spatially combined using beam splitters and then propagate over 1 m in free-space. At the receiver end, the combined branches, each with a different OAM value, are demultiplexed using SLMs, and each OAM beam is converted into a Gaussian-like beam ($\ell = 0$). Each of the four beams is then coupled into an SMF for signal detection and data recovery. Figure 2(b) depicts the detection schemes for OAM-based data encoding. The four channels are detected and simultaneously recorded for offline digital signal processing. The bit information is recovered by: (i) identifying the transmitted OAM mode for each symbol period by calculating the power of each branch and (ii) determining the bit information using the mapping relation $\ell_1 \rightarrow “00,” \ell_2 \rightarrow “01,” \ell_3 \rightarrow “11,” \text{ and } \ell_4 \rightarrow “10.”$ For channel hopping, a 100 Gbit/s QPSK coherent receiver is used to recover the data stream for each branch sequentially.

Figures 3(a) and 3(b) present the normalized waveforms (a1–a5) and eye diagrams (b1–b4) for the four output branches of the switch operating at 10 GHz. The combined waveform verifies that light is routed to only one of the branches in each 100 ps period. Figures 3(c) and 3(d) depict the received normalized waveforms of 10 GHz data encoding when using mode sets $\{-3, -1, +1, +3\}$ with $\Delta = 2$ (c1–c5) and $\{0, +1, +2, +3\}$ with $\Delta = 1$ (d1–d5). We see that only one OAM mode is active among the four OAM states within each symbol period. The received waveforms of the four modes are aligned in time by adjusting tunable delay lines. The quality of the received waveforms is affected by both switch-induced crosstalk and OAM intermodal crosstalk. In general, smaller mode spacing causes increased modal crosstalk. The crosstalk values for all four modes when transmitting OAM mode sets $\{0, +1, +2, +3\}$ and $\{3, -1, +1, +3\}$ are around -11.2 and

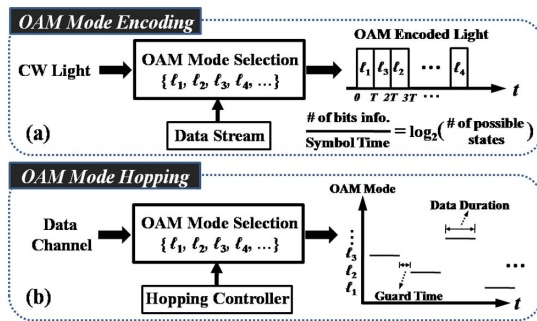


Fig. 1. Concept of (a) data encoding and (b) channel hopping in the spatial domain using OAM modes.

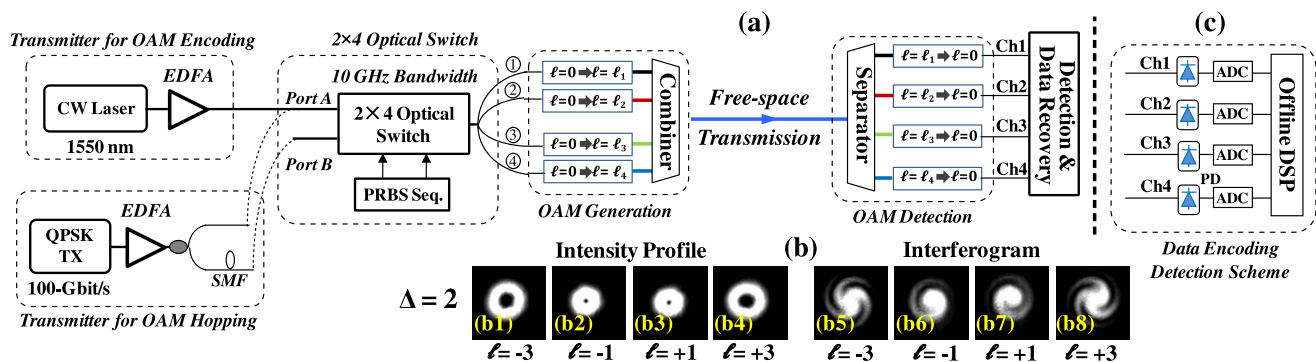


Fig. 2. Schematic overview of the OAM-based data encoding and hopping systems. For mode hopping of 100 Gbit/s data channel, Ports A and B are connected to the two output ports of the OAM hopping transmitter. ADC, analog-to-digital converter; Ch, channel; CW, continuous wave; DSP, digital signal processing; OC, optical coupler; PD, photodiode; Seq., sequence; TX, transmitter.

-18.3 dB, respectively. We see that the waveforms exhibit better quality when using mode set $\{-3, -1, +1, +3\}$, as shown in Fig. 3(c), due to less OAM intermodal crosstalk.

Figure 4(a) shows the overall interference as a function of transmitted power for different mode spacing $\Delta = 1, 2, 3$, and 4. The average interference is obtained as follows: (i) calculating the interference within each symbol period via dividing the power of other OAM modes by the power of the active mode and (ii) averaging the interference values over the entire recorded time. For $\Delta = 3$ and $\Delta = 4$, mode sets $\{-4, -1, +1, +4\}$ and $\{-6, -2, +2, +6\}$ are used, and the measured intermodal crosstalk between modes are around -19.9 and -27.3 dB for all four modes, respectively. We observe that the average interference generally decreases as the transmitted power increases. The $\Delta = 1$ case has larger interference, and interference decreases as the mode spacing increases. Figure 4(b) shows BER curves for 10 GHz data encoding as a function of average interference under different mode spacing. The power penalty of $\Delta = 1$ case is estimated to be 3.2 dB with respect to the $\Delta = 3$ case at the forward error correction (FEC) limit of 3.8×10^{-3} . Given that four OAM states are used, a 20 Gbit/s ($10 \times \log_2 4$) data rate is achieved.

We then investigate the influence of the relative delay between channels, namely time alignment, on the performance of the encoding system. We intentionally adjust the delay of channel ℓ_3 with respect to other three channels (ℓ_1, ℓ_2 , and ℓ_4) using a tunable delay line. This not only affects the determination of ℓ_3 mode (bits "11" according to the mapping

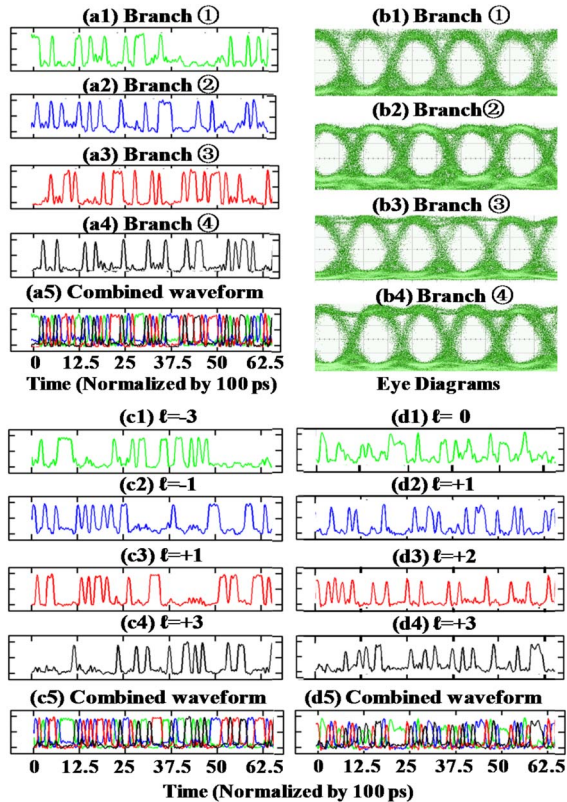


Fig. 3. (a1–a5) Normalized waveforms and (b1–b4) eye diagrams of the four switch output branches at the transmitter. (c1–c5) Received normalized waveforms when using mode set $\{-3, -1, +1, +3\}$ and (d1–d5) using mode set $\{0, +1, +2, +3\}$ with $\Delta = 1$. The symbol period is 100 ps.

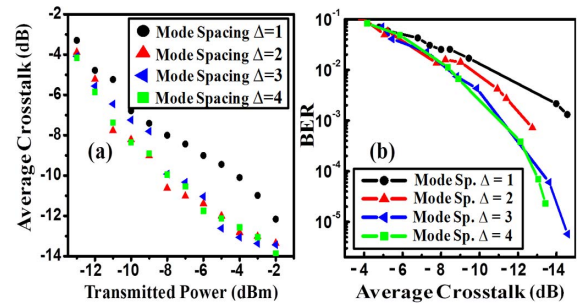


Fig. 4. (a) Measured average interference of the received signals as a function of transmitted power and (b) measured BERs of 20 Gbit/s data encoding when using mode sets with spacing $\Delta = 1, 2, 3$, and 4.

relation) but also introduces interference for the detection of other modes. Figure 5 shows BERs as a function of the time misalignment of channel ℓ_3 under different mode spacing Δ . The transmitted power is fixed at -2 dB. We see that in general, BERs increase rapidly with the delay and become relatively flat for larger time misalignments. For $\Delta = 1, 2, 3$, and 4, BERs exceed the FEC limit of 3.8×10^{-3} at misalignments of around 11, 24, 26, and 47 ps, respectively.

For channel hopping, Port A is disconnected and one 100 Gbit/s QPSK signal is fed into Port B. In this case, the QPSK channel for one user hops between four OAM modes. Figures 6(a1) and 6(a2) show received one-period waveforms for OAM $\ell_3 = +1$ (Ch 3) at hopping rates of 10 and 50 MHz when using mode set $\{-3, -1, +1, +3\}$. Figures 6(a3) and 6(a4) depict the recovered constellations of the 100 Gbit/s QPSK signal during the effective data period and the switch transition time at the 50 MHz hopping rate, respectively. In Fig. 6(a4), we observe that the QPSK constellation during the switch transition time becomes blurred as compared with Fig. 6(a3). This is primarily due to the switching crosstalk when hopping to another mode. Note that for simplification, no blank symbol is inserted into the transmitted QPSK data. The received waveforms during the guard time, which is set to be 10% of the period time in our experiment for ease of BER measurement, are dropped to facilitate evaluation of system performance.

Figure 7 presents the measured BER curves as a function of optical signal-to-noise ratio (OSNR) for channel $\ell_3 = +1$ (Ch3) under different mode spacing and BERs for other channels ($\ell_1 = -3, \ell_2 = -1, \ell_4 = +3$) under $\Delta = 2$. OSNR penalties of 5.1, 2.7, and 2.6 dB are observed for mode spacing of $\Delta = 1, 2$, and 3, respectively. The measured BER curves at

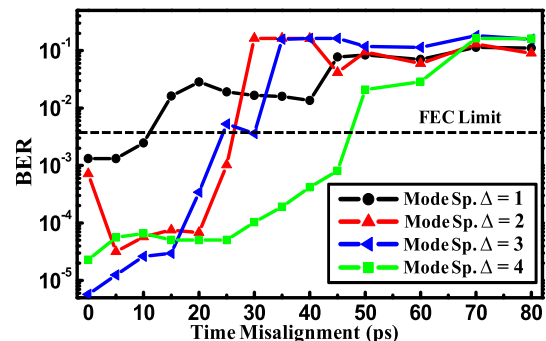


Fig. 5. Measured BERs as a function of time misalignment of channel ℓ_3 when using different mode sets with $\Delta = 1, 2, 3$, and 4.

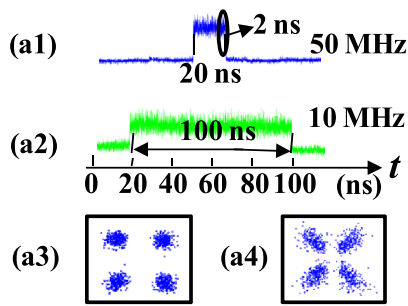


Fig. 6. One period of the received waveforms for channel $\ell_3 = +3$ at hopping rates of (a1) 10 MHz and (a2) 50 MHz. (a3) Recovered 100 Gbit/s QPSK constellations for channel $\ell_3 = +3$ during the data period and (a4) hopping transition time at 50 MHz hopping rate (2 ns guard time). Mode set $\{-3, -1, +1, +3\}$ with $\Delta = 2$ is used.

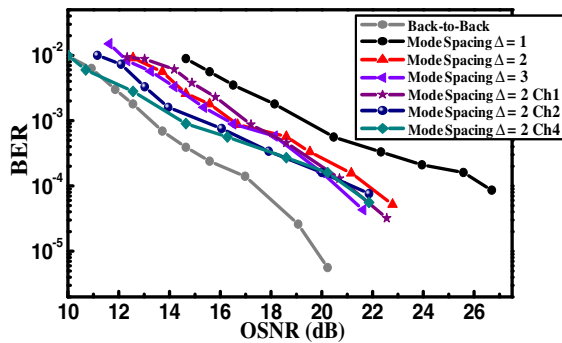


Fig. 7. (Ch3) Measured BERs for channel $\ell_3 = +3$ when using different mode sets with $\Delta = 1, 2,$ and $3,$ and (Ch1, 2, and 4) BERs for other channels when $\Delta = 2$ at 10 MHz hopping rate.

different hopping rates of 1, 10, and 50 MHz while using mode set $\{-3, -1, +1, +3\}$ are shown in Fig. 8. For 50 MHz hopping, a guard time of 2 ns is considered to evaluate BERs. We see that the OSNR penalties for 1, 10, and 50 MHz hopping rates with respect to the back-to-back case (bypassing the link setup) at the FEC limit are below 5.3 dB. This might result from the crosstalk during the switching transition time, and a fast hopping rate causes high switching crosstalk. The BERs for

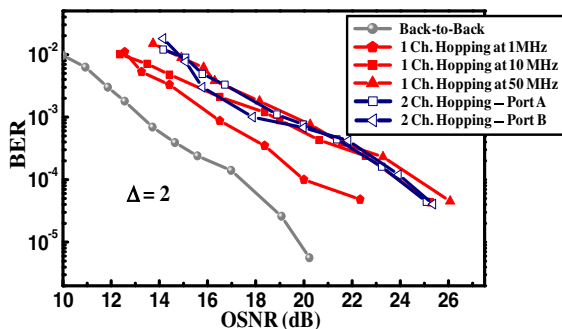


Fig. 8. Measured BERs for one user channel hopping at different rates of 1, 10, and 50 MHz (with guard time of 100, 10, and 2 ns, respectively), and BERs for two user channels hopping at 10 MHz when using mode set $\{\ell = -3, -1, +1, +3\}$.

two user channels hopping at 10 MHz are also shown, in which the other QPSK signal is fed into Port A. The OSNR power penalties for QPSK channels from Ports A and B are 4.8 and 5.7 dB, respectively.

Funding. Air Force Office of Scientific Research (AFOSR); National Science Foundation (NSF); NxGen Partners; Office of Naval Research (ONR).

Acknowledgment. We thank Drs. Michael Kendra and Tommy Willis for fruitful discussions.

REFERENCES

- D. J. Richardson, J. M. Fini, and L. E. Nelson, *Nat. Photonics* **7**, 354 (2013).
- L. E. Nelson, M. D. Feuer, K. Abedin, X. Zhou, T. F. Taunay, J. M. Fini, B. Zhu, R. Isaac, R. Harel, G. Cohen, and D. M. Marom, *J. Lightwave Technol.* **32**, 783 (2014).
- D. Qian, E. Ip, M. Huang, M. Li, A. Dogariu, S. Zhang, Y. Shao, Y. Huang, Y. Zhang, X. Cheng, Y. Tian, P. Ji, A. Collier, Y. Geng, J. Linares, C. Montero, V. Moreno, X. Prieto, and T. Wang, in *Frontiers in Optics* (2012), paper FW6C.3.
- R. G. H. van Uden, R. Amezcua Correa, E. A. Lopez, F. M. Huijskens, C. Xia, G. Li, A. Schülzgen, H. de Waardt, A. M. J. Koonen, and C. M. Okonko, *Nat. Photonics* **8**, 865 (2014).
- J. Wang, J.-Y. Yang, I. M. Fazal, N. Ahmed, Y. Yan, H. Huang, Y. Ren, Y. Yue, S. Dolinar, M. Tur, and A. E. Willner, *Nat. Photonics* **6**, 488 (2012).
- T. Chikama, S. Watanabe, T. Naito, H. Onaka, T. Kiyonaga, Y. Onoda, H. Miyata, M. Suyama, M. Seino, and H. Kuwahara, *J. Lightwave Technol.* **8**, 309 (1990).
- R. Y. Mesleh, H. Haas, S. Sinanović, C. WookAhn, and S. Yun, *IEEE Trans. Veh. Technol.* **57**, 2228 (2008).
- B. Stern, X. Zhu, C. P. Chen, L. D. Tzuang, J. Cardenas, K. Bergman, and M. Lipson, *Optica* **2**, 530 (2015).
- L. Tancevski and I. Andonovic, *J. Lightwave Technol.* **14**, 2636 (1996).
- H. Fathallah, L. A. Rusch, and S. LaRochelle, *J. Lightwave Technol.* **17**, 397 (1999).
- M. D. Audeh, J. M. Kahn, and J. R. Barry, *IEEE Trans. Commun.* **44**, 654 (1996).
- W. O. Popoola, E. Poves, and H. Haas, *J. Lightwave Technol.* **30**, 2948 (2012).
- I. B. Djordjevic, M. Arabaci, L. Xu, and T. Wang, *Opt. Express* **19**, 6845 (2011).
- M. Mirhosseini, O. S. Magaña-Loaiza, M. N. O'Sullivan, B. Rodenburg, M. Malik, M. P. J. Lavery, M. J. Padgett, D. J. Gauthier, and R. W. Boyd, *New J. Phys.* **17**, 033033 (2015).
- L. Allen, M. W. Beijersbergen, R. J. C. Spreeuw, and J. P. Woerdman, *Phys. Rev. A* **45**, 8185 (1992).
- G. Gibson, J. Courtial, M. Padgett, M. Vasnetsov, V. Pas'ko, S. Barnett, and S. Franke-Arnold, *Opt. Express* **12**, 5448 (2004).
- J. Carpenter, B. Thomsen, and T. D. Wilkinson, *European Conference and Exhibition on Optical Communication* (2012), paper Th.2.D.3.
- N. Bozinovic, Y. Yue, Y. Ren, M. Tur, P. Kristensen, H. Huang, A. E. Willner, and S. Ramachandran, *Science* **340**, 1545 (2013).
- H. Huang, G. Milione, M. P. J. Lavery, G. Xie, Y. Ren, Y. Cao, N. Ahmed, T. Nguyen, D. A. Nolan, M.-J. Li, M. Tur, R. R. Alfano, and A. E. Willner, *Sci. Rep.* **5**, 14931 (2015).
- I. B. Djordjevic, *Opt. Express* **19**, 14277 (2011).
- M. Mirhosseini, O. S. Magana-Loaiza, C. Chen, B. Rodenburg, M. Malik, and R. W. Boyd, *Opt. Express* **21**, 30196 (2013).
- N. P. Diamantopoulos, M. Hayashi, Y. Yoshida, A. Maruta, R. Maruyama, N. Kuwaki, K. Takenaga, H. Uemura, S. Matsuo, and K. Kitayama, *Opt. Express* **23**, 23660 (2015).